JOM, Vol. 65, No. 3, 2013
DOI: 10.1007/s11837-012-0529-4

Twinning in Strained Ferroelastics: Microstructure and Statistics

X. DING,[1,2,4] T. LOOKMAN,[2] E. K. H. SALJE,[3] and A. SAXENA[2]

1.—State Key Laboratory for Mechanical Behavior of Materials, Xi'an Jiaotong University, Xi'an 710049, People's Republic of China. 2.—Theoretical Division, Los Alamos National Laboratory, Los Alamos, NM 87545, USA. 3.—Department of Earth Sciences, University of Cambridge, Cambridge CB2 3EQ, UK. 4.—e-mail: dingxd@mail.xjtu.edu.cn

The generation of functional interfaces such as superconducting and ferroelectric twin boundaries requires new ways to nucleate as many interfaces as possible in bulk materials and thin films. Materials with high densities of twin boundaries are often ferroelastics and martensites. In this review, we show that the nucleation and propagation of twin boundaries depend sensitively on temperature and system size. Sudden changes of the domain pattern manifest themselves as avalanches or "jerks" in the potential energy of the sample. At high temperatures, the change of the twin pattern is thermally activated; the probability P to find sudden energy changes of jerks E follows the Vogel–Fulcher statistics $P(E) \sim \exp(E/(T - T_{VF}))$, whereas the athermal regime at low temperatures corresponds to power-law statistics $P(E) \sim E^{-\varepsilon}$. We find that the complexity of the pattern is well characterized by the number of junctions between twin boundaries. Materials with soft bulk moduli have much higher junction densities than those with hard bulk moduli. Soft materials also show an increase in the junction density with diminishing sample size. The change of the complexity and the number density of twin boundaries represents an important step forward in the development of "domain boundary engineering," where the functionality of the materials is directly linked to the domain pattern.

INTRODUCTION

An active field of research in materials science has centered on understanding the behavior of ferroelastic interfaces, especially if they can be made to acquire properties that are quite distinct from those of the bulk materials in which they reside.[1–13] The interfaces can be superconducting in an otherwise insulating bulk crystal, have high ionic mobilities, or show chiral properties. For example,[1,2,14–16] the introduction of Na ions or oxygen vacancies in the twin walls of tungsten trioxide, WO_3, dramatically changes its conductivity so that it becomes a superconductor at 3 K. The dopants follow the trajectory of the twin walls, but it is the change in composition from WO_3 to $WO_{2.95}$ that induces a metal–insulator transition and at low temperatures leads to a drop in resistance. For such applications and domain engineering in general, it is highly desirable to have a high density of twin walls that can, for example, facilitate read and write functions from dense arrays of ferroelectric twins.[17] We shall discuss here how straining ferroelastic crystals with desired material and physical properties can provide a means of increasing twin wall densities. This is in contrast to the conventional approach that involves quenching from the high-temperature parent phase down to room temperature to generate a metastable state that then slowly evolves to a ferroelastic phase.

A second aspect of our work is examining the twin boundary motion and subsequent microstructure formation and how it relates to the statistical and mechanical properties of the response. The issue of jerky or avalanche behavior is also well known in magnetic systems where Barkhausen noise[18,19] is generated by pinning and depinning (and subsequent relaxation) of magnetic domains. Our focus here will be on demonstrating how thermal activation in a driven system can lead to behavior far richer than the power law distributions in energy in athermal regimes typically studied in ferroelastic martensites by acoustic emission[5,20–23] or the dislocation plasticity in nanopillars.[24–26] We will show

(Published online January 3, 2013)

that the energy distributions span from power law to Vogel–Fulcher behavior as a function of temperature.[27–29] A stretched exponential describes the distribution of stress in the crossover regime.[30]

The outline of this work is the following. In the "Ferroelastic Transitions and Experimental Progress" section, we introduce ferroelastics and review the experimental work that has so far been performed. Much of this has been focused on thin films on substrates with measurements of heat flux or acoustic emission to track bursts or avalanches. Dynamical mechanical analyses (DMAs) have monitored the propagation of needle domains, the preferred mechanism when the external driving force is small. The bursts are signatures of relaxation as the interfaces overcome pinning because of defects or other heterogeneities in the system. The distribution of frequency of bursts versus burst strength shows power-law behavior at low temperatures. In the "Atomistic Simulations of Twin Boundary Propagation and Microstructure" section, we introduce our atomistic simulations that are the basis of the dual focus of this review, namely, how shear straining a crystal can lead to dense twin walls with a large fraction of intersecting twins or "junction" densities, and how distributions other than power-law behavior become important as the temperature increases. In the "Statistical Nature of Twin Boundary Microstructure: Distributions and Effects of Temperature" section, we discuss our results within the context of a temperature phase diagram which shows the different regimes that are accessible, from power law to stretched exponential to Vogel–Fulcher behavior. We conclude with a brief outlook of future directions.

FERROELASTIC TRANSITIONS AND EXPERIMENTAL PROGRESS

Ferroelastic materials undergo structural phase transitions from a paraelastic phase to a ferroelastic phase via a second-order or first-order transformation and display elastic hysteresis behavior in the ferroelastic phase. There is normally a group–subgroup relationship between the parent paraelastic phase and the product ferroelastic phase and their variants.[31,32] The domain wall or twin boundary between the product variants is a mirror plane with a small shear angle, typically $<4°$, and is quite "rounded" and often diffused with a layer or more of the parent phase (or some other, structurally similar phase).[33] The boundary is therefore not atomistically sharp, in contrast to deformation twins in nonferroelastic materials, which can have large shear angles (e.g., 30°) and are quite sharp.[34–39] The twin boundary generally has a less dense structure than the bulk and serves as a sink for defects or vacancies. This "doping" of twin boundaries can lead to very different functional properties of the walls compared with the bulk. Figure 1a[31] shows typical domain structure in $Pb_3(PO_4)_2$ and Fig. 1b is high-resolution transmission electron microscopy (HRTEM) image of a domain boundary that is six unit cells thick.[14] Figure 1c shows how one can traverse continuously from one variant to the other via the twin boundary.[33]

Ferroelastic switching relates to overcoming local energy barriers from one variant to another. The external control parameter is either the applied stress (soft boundary conditions) or the predescribed strain of the sample (hard boundary conditions). If heterogeneities are present, then the global energy landscape becomes rugged with a series of metastable states in a complex microstructure. The heterogeneities can originate from extrinsic defects or can be the result of domain boundary jamming where twin boundaries intersect and form junctions which impede the further easy movement of the boundaries. When the system is driven, for example by shear, it will change from one minimum to another in a series of discrete jumps. These jumps or jerks appear as peaks in an "energy versus shear" spectrum. The jerks can be measured by acoustic emission, dynamical mechanical analyzer measurements, resonant acoustic spectroscopy, or other techniques (e.g., measurement of heat fluxes or needle domain tip movement) in shape memory alloys and related materials.[3,14,20–23,40,41] The distribution of jerk energies $P(E)$ often follows a power law behavior $P(E) \sim E^{-\varepsilon}$ with exponents between -1.3 and -2. The power-law behavior is quite ubiquitous as it has been observed in a number of functional material systems other than ferroelastics. These include the sudden bursts in magnetization known as Barkhausen noise in magnetic systems containing Fe, Ni, and Co,[42] and the changes in magnetic flux leading to vortex avalanches in superconducting materials such as NbTi.[43]

Currently, experiments on ferroelastics are performed by quenching from a high-temperature, high-symmetry austenite or tweed phase to temperatures well into the ferroelastic phase—this has been used since ferroelastics were first discovered.[44–46] It is the reverse process of very slow cooling whenever twinning needs to be avoided. Fast quenching can lead to twin wall densities of the order of 2.8% of the total number of atoms.[47] The structure is quite metastable and small thermal fluctuations will modify the microstructure of the ferroelastic phase. An alternative route to produce high twin boundary densities is to shear the crystal in the ferroelastic phase. Here, a film is deposited in the high-temperature phase onto a substrate and cooled to room temperature. The substrate is chosen so that it induces a shear of the film. When the shear exceeds the yield shear strain, the ferroelastic film twins dramatically giving rise to a multivariant microstructure.[27] Figure 2a shows an YBCO film that is in the checker-board tweed phase at high temperatures. When quenched to low temperature,

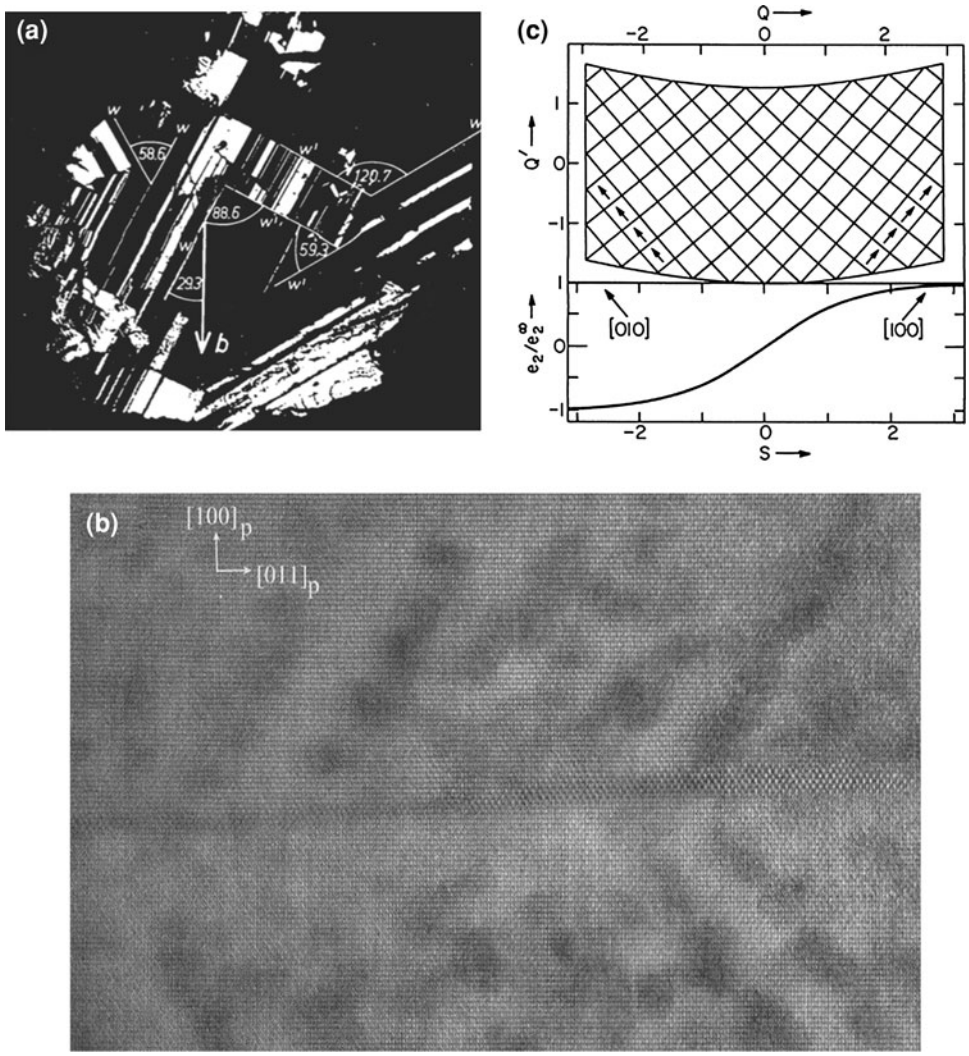

Fig. 1. (a) Typical domain structure in $Pb_3(PO_4)_2$ with compatibility angles near 30, 60, 90 and 120°. The wall type *W* and *W'* are annotated. The vector *b* indicates the monoclinic *b*-axis of the large domain in the center of the figure (from Ref. 32). (b) HRTEM of a domain boundary that is six unit cells thick (from Ref. 15). (c) How one can traverse continually from one variant to the other via the twin boundary (from Ref. 34).

the intersecting twin pattern in the ferroelastic phase forms high density of junctions (Fig. 2b).[46]

ATOMISTIC SIMULATIONS OF TWIN BOUNDARY PROPAGATION AND MICROSTRUCTURE

The experimentally observed evolution of twin structures can be mimicked in computer simulation experiments with some very simple model assumptions. A very successful approach is to use monoatomic structures where the ground state is determined by double well potentials of one key interatomic interaction. Figure 3 shows the potential and model system adopted in Refs. 27–30. The ground state corresponds to one of the potential minima and is directly connected to the shear angle of the crystal. We choose this angle so that the ground state is a slightly sheared pseudocubic lattice and the length scales of the interfaces or twin walls are of the order of three atomic units. We take the shear angle to be 4°—typically below that of martensitic materials with shear angles of ~8–10° but slightly larger than for most ferroelastic oxides. The shear angle is controlled by the diagonal or next nearest neighbor springs. The nearest neighbor springs control the bulk modulus (we will compare below "hard" and "soft" materials; see Ref. 28 for the exact definition of these terms) and transition temperature. The third next-nearest-neighbor springs control the thickness of the twin boundary and the twin density. The thicknesses of the interface and surface relaxations are determined by the competition between nearest-neighbor and next-nearest-neighbor (vertical) springs. The initial conditions contain one horizontal twin boundary in the middle and the system is allowed to relax completely. The

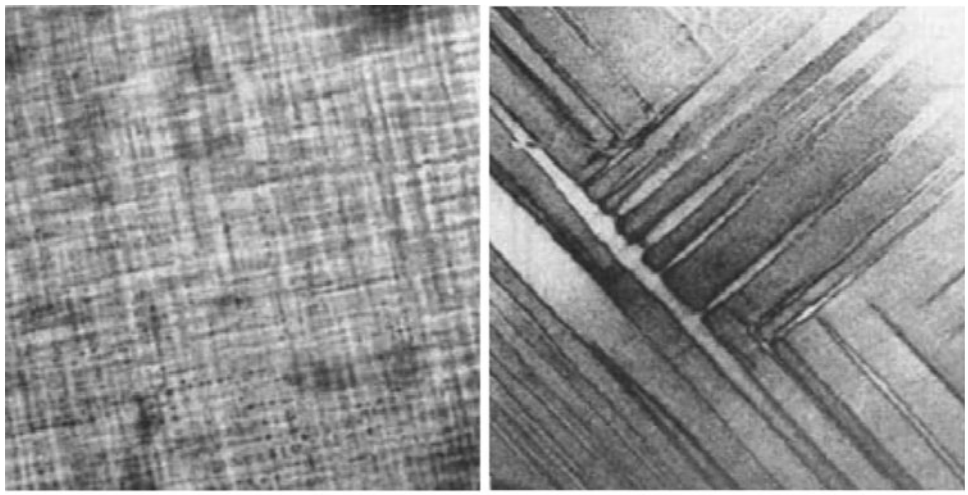

Fig. 2. (a) YBCO film that is in the checker-board tweed phase at high temperatures. When quenched to low temperature, the intersecting twin pattern in the ferroelastic phase forms junctions (b) (from Ref. 47).

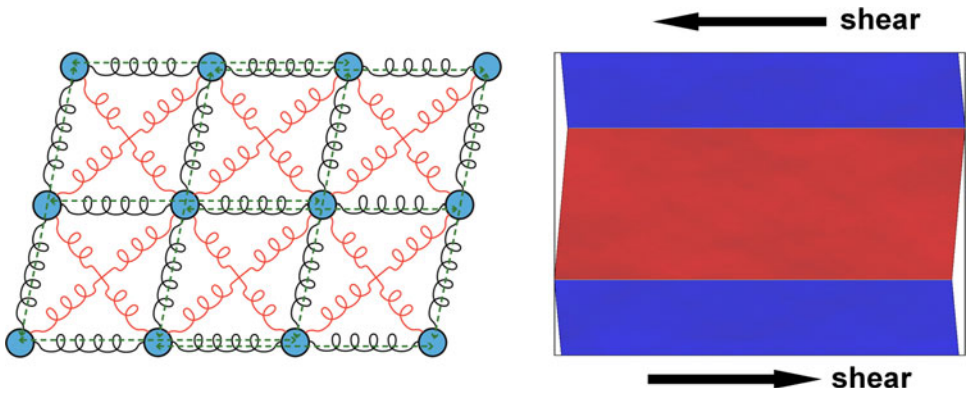

Fig. 3. The potential and model system we adopt. The role of the interatomic potentials is discussed in the text.

ground state is sheared with an angle less than 4°, but the surface relaxations bring it up to 4°. We also have two buffer layers to transmit the shear to the atoms to allow the dissipation of load energy. This mimics the action of a clamp.

Using an initial condition as shown in Fig. 3 with two horizontal twin boundaries, shearing in the directions shown leads to the formation of a dynamic tweed structure with a local cross-hatched pattern. Figure 4 shows the integrated potential energy (related to the average stress) versus applied shear strain. Elastic energy is pumped into the system until at point A the system yields and the energy drops to point B. The microstructure at point B is a multivariant twin structure with a relatively high density of twin intersections. This structure transforms on further shearing to a uniform single domain at point C. The domain pattern at B after the yield point is quite sensitive to changes in the bulk modulus as well as the system size. Figure 5 compares the domain pattern from a hard (left

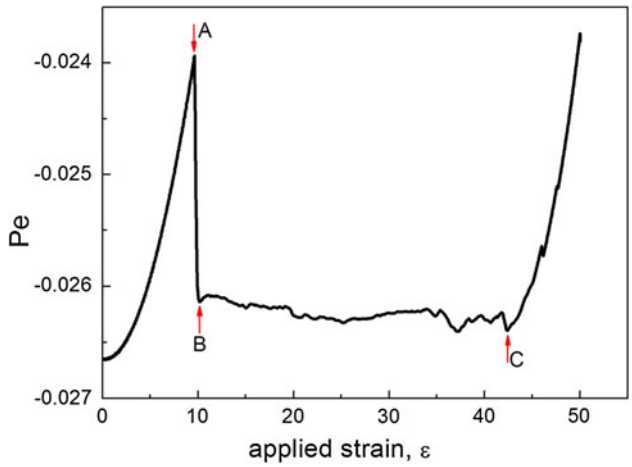

Fig. 4. The integrated potential energy (related to the average stress) versus applied strain. Point A is the upper yield point and point B is the lower yield point at which a multivariant twin structure is obtained. On further shearing, the system goes to a single domain state at point C.

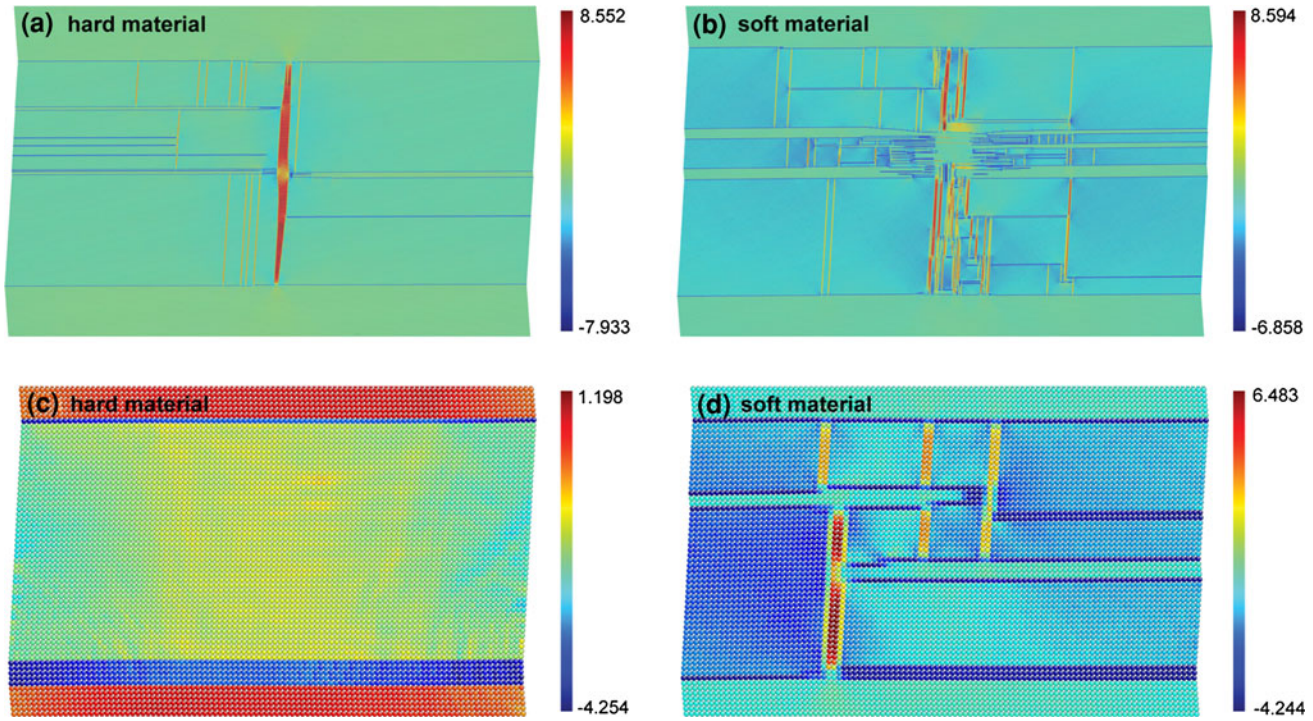

Fig. 5. Comparison of the domain pattern from a hard (left panels) to a soft (right panels) material, as well as the response from a large system containing 641,600 atoms (upper panels) to one containing 10,200 atoms (lower panels).

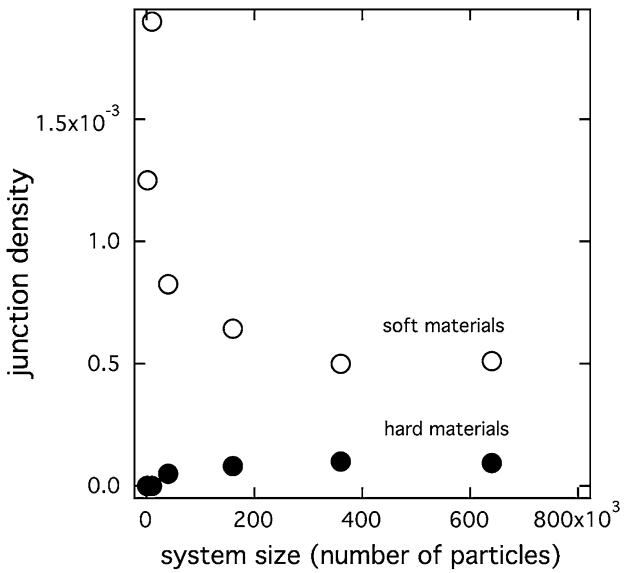

Fig. 6. Junction densities for hard and soft materials as a function of system size. Soft materials always possess higher junction densities which increase with decreasing system sizes.

panels) to a soft (right panels) material, as well as the response from a large system containing 641,600 atoms (upper panels) to one containing 10,200 atoms (lower panels). We can see a small number of vertical domains and few horizontal domains for the hard, large system. The corresponding soft system has a much more complex pattern with a large number of horizontal and vertical twins. This network, which is still present to a limited extent for the small, soft material, is destroyed as the stable domain invades the unstable region in the hard case. No vertical walls in a small system of hard material are seen.

A convenient parameter that provides a measure of the complexity of the pattern is the junction density. A junction is defined as the intersection of twin boundaries and can easily be calculated in a simulation as the number of atoms displaced in a junction divided by the total number of atoms in the simulation (no periodic boundary conditions). The junction density is plotted in Fig. 6 for hard and soft materials as a function of system size. The hard system has fewer junctions (10^{-4}) than the soft system (10^{-3}). The increase for soft systems is a result of the strong structural relaxation around junctions. This result shows that the desired properties of high-junction densities are best achieved for soft materials and that a small system size does not impede the formation of twin walls. The junction density has been experimentally measured in very few cases. We estimate that in large, soft materials it can reach about 5% of the total volume, which is consistent with 2.8% found experimentally in Co-doped YBCO.[47]

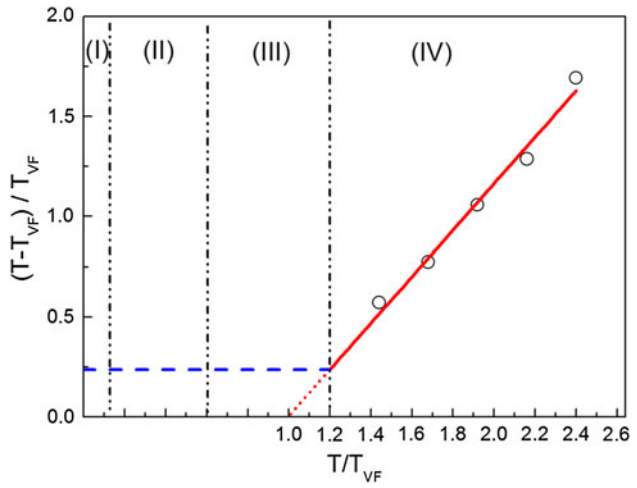

Fig. 7. Phase diagram of the distribution functions for the pattern formation as a function of temperature. At low temperatures, the distribution of the jerky behavior is sparse and probability $P(E)$ to find a "jerk" with an energy E is not power-law distributed (regime I). At moderate temperatures, the process is athermal and follows a power law distribution $P(E) \sim E^{-\varepsilon}$ (regime II). At temperatures above the Vogel–Fulcher temperature T_{VF}, the pattern evolution is thermally activated and $P(E)$ follows Vogel–Fulcher statistics (regime IV). At the temperatures between power-law and Vogel–Fulcher regime, we find $P(E)$ follows stretched exponential statistics (regime III).

STATISTICAL NATURE OF TWIN BOUNDARY MICROSTRUCTURE: DISTRIBUTIONS AND EFFECTS OF TEMPERATURE

The study of distributions of energy jerks has previously involved systems with intrinsic defects that provide pinning forces that naturally lead to multiple energy minima and jerky behavior. The power law distribution is ubiquitously seen and is obtained for athermal behavior, without any temperature dependence. This raises the question of whether one needs athermal behavior for power law statistics and how it changes in the presence of temperature or thermal activation. It is this aspect that we focus on in this section. However, we first review the behavior at relatively low temperatures where thermal activation is negligible.

Starting from an initial condition with one twin boundary in the center of the crystal at low temperatures, shearing the system very slowly leads to nucleation and propagation of twins from the free surfaces on either side. This solitary wave motion of needle twins has been previously well characterized. The kink solutions have the standard form $Q(r,t) = Q_0 \tanh(r - vt)/\left[w\left(1 - v^2/c_0^2\right)^{1/2}\right]$, where $2w$ is the twin wall thickness at initial zero velocity, $v = 0$, and c_0 is a characteristic velocity. The time evolution of the potential energy shows a saw-tooth behavior that indicates the buildup and release of elastic energy as a function of applied strain. The distribution of the jerky behavior is sparse and not power-law distributed (Fig. 7, regime I). At moderate temperatures, we begin to see the role of structural disorder in the microstructure. The initial nucleation and propagation of needle domains leads to the formation of new domains that provide the nucleation sites for the formation of vertical needle twins. Subsequently, the main horizontal twins move down as solitary wave motion. This motion involves pinning and depinning at sites that are the intersection of horizontal and vertical twins. Continued shearing leads to a uniform single-domain state. The time evolution of the potential energy is similar to that at low temperature. The probability of the peak values of the energy derivative $(\mathrm{d}pe/\mathrm{d}\varepsilon)^2$ depends on $(\mathrm{d}pe/\mathrm{d}\varepsilon)^2$ at moderate temperatures as a power-law behavior $p(E) \sim E^{-2}$ (Fig. 7, regime II). At higher temperatures, where there is greater thermal activation, we see that the previous power-law changes to a Vogel–Fulcher behavior ($P(J) \sim \exp(E/(T - T_{VF}))$, where T_{VF} is the Vogel–Fulcher temperature, that is the threshold temperature for thermal activation, see Refs. 28–31 for details (Fig. 7, regime IV). The Vogel–Fulcher temperature relates to the thermal crossover point below which we obtain power-law behavior and above which the system is thermally activated. An interesting aspect is what happens at intermediate temperatures where the system neither obeys power-law statistics nor the Vogel–Fulcher behavior. Here, we find that in this cross-over regime, a stretched exponential of the form $P(E) \sim E^{-\varepsilon} \exp -(E/E_0)^n$, where $\varepsilon \approx 0$ and $n = 0.4$ fits the data well[30] (Fig. 7, regime III).

SUMMARY AND FUTURE DIRECTIONS

Our focus has been to show how starting from a single crystal, we can generate heterogeneities such as twin walls and intersections by driving the system by means of a deformation mode, such as shearing. We have demonstrated that this allows us to generate high densities of twin walls and junctions and thus provides an alternative, experimental means to fabricating such arrays and junctions than quenching from a high temperature. We have provided some guidance as to what are desirable material properties, such as small bulk modulus and system sizes, to optimize twin junctions. We have also shown that the statistics of jerky behavior changes from the typical power-law behavior at low temperatures to stretched exponential at intermediate temperatures and Vogel–Fulcher at high temperatures. Figure 7 depicts how all these results may be collected in a temperature phase diagram that shows the different regimes of behavior as a function of temperature.

Future challenges include the behavior in the presence of defects as well as varying the strain rate of deformation. The strain rates we have used so far have been very low. In addition, although we characterized the process and the distributions, there is

a need for a model to capture the essential physics of structural disorder competing with thermal activation to predict the changes in the distributions we have seen.

ACKNOWLEDGEMENTS

This work was supported in part by NSFC (51171140, 51231008), the 973 Program of China (2010CB631003, 2012CB619402), 111 project (B06025), and U.S. Department of Energy at LANL (DE-AC52-06NA25396). E.K.H.S. is grateful to the Leverhulme Foundation for support.

REFERENCES

1. A. Aird and E.K.H. Salje, *J. Phys.: Condens. Matter* 10, L377 (1998).
2. Y. Kim, M. Alexe, and E.K.H. Salje, *Appl. Phys. Lett.* 96, 032904 (2010).
3. J. Seidel, P. Maksymovych, Y. Batra, A. Katan, S.Y. Yang, Q. He, A.P. Baddorf, S.V. Kalinin, C.-H. Yang, J.-C. Yang, Y.-H. Chu, E.K.H. Salje, H. Wormeester, M. Salmeron, and R. Ramesh, *Phys. Rev. Lett.* 105, 197603 (2010).
4. M. Calleja, M.T. Dove, and E.K.H. Salje, *J. Phys.: Condens. Matter* 15, 2301 (2003).
5. A. Ohtomo and H.Y. Hwang, *Nature* 427, 423 (2004).
6. S.A. Pauli, S.J. Leake, B. Delley, M. Björck, C.W. Schneider, C.M. Schlepütz, D. Martoccia, S. Paetel, J. Mannhart, and P.R. Willmott, *Phys. Rev. Lett.* 106, 036101 (2011).
7. M. Huijben, G. Rijnders, D.H.A. Blank, S. Bals, S. Van Aert, J. Verbeeck, G. Van Tendeloo, A. Brinkman, and H. Hilgenkamp, *Nat. Mater.* 5, 556 (2006).
8. G. Herranz, M. Basletić, M. Bibes, C. Carrétéro, E. Tafra, E. Jacquet, K. Bouzehouane, C. Deranlot, A. Hamzić, J.-M. Broto, A. Barthélémy, and A. Fert, *Phys. Rev. Lett.* 98, 216803 (2007).
9. B. Kalisky, J.R. Kirtley, J.G. Analytis, J.-H. Chu, I.R. Fisher, and K.A. Moler, *Phys. Rev. B* 83, 064511 (2011).
10. Y. Ivry, D. Chu, J.F. Scott, E.K.H. Salje, and C. Durkan, *Nano Lett.* 11, 4619 (2011).
11. T. Birol, N.A. Benedek, and C.J. Fennie, *Phys. Rev. Lett.* 107, 257602 (2011).
12. A. Lubk, S. Gemming, and N.A. Spaldin, *Phys. Rev. B* 80, 104110 (2009).
13. T. Lottermoser and M. Fiebig, *Phys. Rev. B* 70, 220407 (2004).
14. E.K.H. Salje, *ChemPhysChem* 11, 940 (2010).
15. S.V. Aert, S. Turner, R. Delville, D. Schryvers, G.V. Tendeloo, and E.K.H. Salje, *Adv. Mater.* 24, 523 (2012).
16. W.T. Lee, E.K.H. Salje, L. Goncalves-Ferreira, M. Daraktchiev, and U. Bismayer, *Phys. Rev. B* 73, 214110 (2006).
17. X.F. Wu, K.M. Rabe, and D. Vanderbilt, *Phys. Rev. B* 83, 020104 (2011).
18. J.S. Urbach, R.C. Madison, and J.T. Markert, *Phys. Rev. Lett.* 75, 276 (1995).
19. K.A. Dahmen, J.P. Sethna, M.C. Kuntz, and O. Perkovic, *J. Magn. Magn. Mater.* 226, 1287 (2001).
20. E. Vives, J. Ortin, L. Manosa, L. Rafols, R. Perez-Magrane, and A. Planes, *Phys. Rev. Lett.* 72, 1694 (1994).
21. F.J. Perez-Reche, E. Vives, L. Manosa, and A. Planes, *Phys. Rev. Lett.* 87, 195701 (2001).
22. F.J. Perez-Reche, B. Tadic, L. Manosa, A. Planes, and E. Vives, *Phys. Rev. Lett.* 93, 195701 (2004).
23. F.J. Perez-Reche, F. Casanova, E. Vives, L. Manosa, A. Planes, J. Marcos, X. Batlle, and A. Labarta, *Phys. Rev. B* 73, 014110 (2006).
24. M.-C. Miguel and S. Zapperi, *Science* 312, 1151 (2006).
25. D.M. Dimiduk, C. Woodward, R. LeSar, and M.D. Uchic, *Science* 312, 1188 (2006).
26. K.A. Dahmen, Y. Ben-Zion, and J.T. Uhl, *Phys. Rev. Lett.* 102, 175501 (2009).
27. E. Salje, X. Ding, Z. Zhao, T. Lookman, and A. Saxena, *Phys. Rev. B* 83, 104109 (2011).
28. X. Ding, Z. Zhao, T. Looman, A. Saxena, and E. Salje, *Adv. Mater.* 24, 5385 (2012).
29. E. Salje, X. Ding, Z. Zhao, and T. Looman, *Appl. Phys. Lett.* 100, 222905 (2012).
30. X. Ding, Z. Zhao, T. Looman, J. Sun, A. Saxena, and E. Salje, *Phys. Rev. B*, under review.
31. E.K.H. Salje, *Phase Transitions in Ferroelastic and Co-Elastic Crystals* (Cambridge, UK: Cambridge University Press, 1993).
32. K. Bhattacharya, S. Conti, G. Zanzotto, and J. Zlmmer, *Nature* 428, 55 (2004).
33. G.R. Barsch and J.A. Krumhansl, *Phys. Rev. Lett.* 53, 1069 (1984).
34. J.W. Cahn, Y. Mishin, and A. Suzuki, *Acta Mater.* 54, 4953 (2006).
35. Y. Mishin, A. Suzuki, B.P. Uberuaga, and A.F. Voter, *Phys. Rev. B* 75, 224101 (2007).
36. D.A. Molodov, V.A. Ivanov, and G. Gottstein, *Acta Mater.* 55, 1843 (2007).
37. S. Li, X. Ding, J. Li, X. Ren, J. Sun, and E. Ma, *Nano Lett.* 10, 1774 (2010).
38. S. Li, X. Ding, J. Li, X. Ren, J. Sun, E. Ma, and T. Lookman, *Phys. Rev. B* 81, 245433 (2010).
39. S. Li, X. Ding, J. Deng, T. Lookman, J. Li, X. Ren, J. Sun, and A. Saxena, *Phys. Rev. B* 82, 205435 (2010).
40. M.C. Gallardo, J. Manchado, F.J. Romero, J.D. Cerro, E.K.H. Salje, A. Planes, E. Vives, R. Romero, and M. Stipcich, *Phys. Rev. B* 81, 174102 (2010).
41. R.J. Harrison and E.K.H. Salje, *Appl. Phys. Lett.* 97, 021907 (2010).
42. S. Field, J. Witt, F. Nori, and X. Ling, *Phys. Rev. Lett.* 74, 1206 (1995).
43. L. Carrillo, L. Mañosa, J. Ortín, A. Planes, and E. Vives, *Phys. Rev. Lett.* 81, 1889 (1998).
44. A.M. Bratkovsky, S.C. Marais, V. Heine, and E.K.H. Salje, *J. Phys.: Condens. Matter* 6, 3679 (1994).
45. A.M. Bratkovsky, E.K.H. Salje, S.C. Marais, and V. Heine, *Phase Transit.* 48, 1 (1994).
46. E.K.H. Salje and K. Parlinkski, *Supercond. Sci. Technol.* 4, 93 (1991).
47. W.W. Schmahl, A. Putnis, E.K.H. Salje, P. Freeman, A. Graeme-Barber, R. Jones, K.K. Singh, J. Blunt, P.P. Edwards, J. Loram, and K. Mirza, *Philos. Mag. Lett.* 60, 241 (1989).